

Magneto-Thomson and transverse Thomson effects in an interacting hadron gas in the presence of an external magnetic field

Kamaljeet Singh, Kshitish Kumar Pradhan, and Raghunath Sahoo*

Department of Physics, Indian Institute of Technology Indore, Simrol, Indore 453552, India

(Dated: June 30, 2025)

The universality of electric charge as a quantum number allows thermoelectric properties to manifest across diverse systems, starting from a hot quantum chromodynamics matter in heavy-ion collisions at a high energy scale to semiconductors in condensed matter systems at a low energy scale. In this work, we explore the emergence of magneto-transport phenomena, specifically the magneto-Thomson and transverse Thomson effects, in a hot and dense hadronic medium produced in relativistic heavy-ion collisions at Relativistic Heavy Ion Collider and Large Hadron Collider energies. These phenomena arise due to the combined influence of temperature gradients and non-zero baryon chemical potential, particularly in the presence of an external magnetic field. Using the relativistic Boltzmann transport equation within the relaxation time approximation, we analyze the behavior of the hadronic medium considering different frameworks of hadron resonance gas models. The presence of external magnetic fields breaks the isotropy of the thermoelectric transport coefficient matrix, giving rise to new components of the Thomson coefficient, namely, magneto-Thomson and transverse Thomson coefficients. For the first time, we estimate the magneto-Thomson and transverse Thomson coefficients, which originate from the temperature dependence of the magneto-Seebeck coefficient and Nernst coefficient, respectively, in hadron gas under the influence of a magnetic field. Our findings provide a novel perspective on the higher-order thermoelectric properties of the hot and dense hadronic medium in the context of heavy-ion collisions.

I. INTRODUCTION

Scientific curiosity about the early universe has led to groundbreaking progress in experimental physics, particularly in the study of strongly interacting matter governed by quantum chromodynamics (QCD). Facilities like the Large Hadron Collider (LHC) and the Relativistic Heavy Ion Collider (RHIC) serve as modern laboratories for probing the thermodynamic and transport properties of strongly interacting matter, such as the quark-gluon plasma (QGP) and hot hadron gas [1, 2]. This QGP phase of matter forms at very high temperatures and/or baryon chemical potentials and exists for a short lifetime with an order of a few fermi. As the QGP expands and cools rapidly, it undergoes hadronization, eventually leading to a dense hadron gas that freezes out into detectable subatomic particles. Understanding the properties of this hadronic phase is essential for reconstructing the full evolution of the collision and probing the characteristics of dense nuclear matter. During this evolution, temperature gradients naturally develop in space and time due to the rapid expansion and cooling of the medium from the central collision zone to outward. These spatial and temporal temperature variations significantly influence the dynamics of the system. In the presence of conserved charges, such as baryon number or electric charge, these temperature gradients can drive charge carriers to diffuse along these gradients, leading to the development of thermoelectric currents [3]. These currents lead to the study of thermal and electrical conductivity, particularly relevant in the context of heavy-

ion collisions [4, 5]. In the hadron resonance gas (HRG) medium, the thermal, and charge transport and the interplay between these two gives rise to thermoelectric coefficients, such as the Seebeck [6–8] and Thomson [9–11] coefficients, which characterize the response of the medium to thermal forces. The leading-order coefficient, such as the Seebeck coefficient, in particular, characterizes the ability of a conducting medium to convert thermal gradients into electric potential and is defined under open-circuit conditions where the net electric current is zero [12]. For a number of materials, the Seebeck coefficient is not spatially uniform but instead varies with temperature, giving rise to higher-order thermoelectric effects. When an electric current passes through such a gradient, the system exhibits the Thomson effect, quantified by the Thomson coefficient. This coefficient represents the amount of net heat absorbed or emitted per unit current per unit temperature gradient, with its magnitude and sign dependent on the intrinsic properties of the medium and the directionality of both current flow and thermal gradient [13]. In the domain of high-energy physics, the leading-order thermoelectric properties of a hot and dense hadron gas have been explored through several theoretical frameworks, including relativistic kinetic theory [14–16], hydrodynamic modeling [17–19], and lattice QCD simulations [20, 21]. Understanding these coefficients provides insights into non-equilibrium complex transport phenomena and the microscopic properties of hot QCD matter under extreme conditions.

The dynamics of thermoelectricity is affected by the presence of a nonzero magnetic field because of the experience of the Lorentz force by charge carriers. Peripheral heavy-ion collisions are capable of generating extremely strong magnetic fields as a result of the relativistic motion

* Corresponding Author: Raghunath.Sahoo@cern.ch

of spectator protons. In such events, the magnetic field strength can peak around $m_\pi^2 \sim 10^{18}$ G for Au-Au collisions at RHIC and reach up to $15 m_\pi^2$ in Pb-Pb collisions at the LHC [22, 23]. These fields tend to dissipate almost instantly in a vacuum, but the situation changes when a thermalized conducting medium, such as the quark-gluon plasma, is present. Due to its finite electrical conductivity, the medium supports the induction of secondary magnetic fields aligned with the initial external field, as described by Faraday's law [24]. This results in a slower decay of the magnetic field, allowing it to play a significant role in influencing the complete evolution of the fireball, particularly its thermodynamic and transport properties. The influence of magnetic fields on the conductivity of QCD medium, both electrical and thermal, has been extensively addressed in the literature [4, 25, 26]. Under such magnetic field conditions, leading-order thermoelectric transport becomes directionally dependent, giving rise to the magneto-Seebeck and Nernst coefficients. Unlike the Seebeck coefficient, which responds to longitudinal temperature gradients alone, the Nernst coefficient is a transverse response that emerges only in the presence of magnetic fields. It quantifies the generation of an electric current perpendicular to both the thermal gradient and the magnetic field [12]. Previous studies have analyzed this behavior for the hadronic medium using hadron resonance gas models [14, 16], while the study [27] explores the impact of magneto-thermoelectric effects on conserved charge diffusion. The thermoelectric behavior of the QGP has also been explored in both isotropic [28] and anisotropic [29, 30] media, largely within perturbative QCD formalisms, which are valid at very high temperatures. The temperature dependence of the leading-order thermoelectric coefficients in a magnetic field gives rise to the higher-order thermoelectric coefficients. In our previous study [13], we calculated the Thomson coefficient of interacting hot hadron gas, which originates due to the temperature dependence of the Seebeck coefficient. The Thomson effect can be understood as originating from the simultaneous operation of the Seebeck and Peltier effects [31], and appears when the medium has a temperature dependence of the Seebeck coefficient. If the charge current flows through the spatial gradient of the Seebeck coefficient, the self-induced Peltier effect modulates the temperature in response to the charge current [32]. In the current study, we calculate the Thomson effect for hadron gas in the presence of a magnetic field. The presence of a magnetic field creates an anisotropy in the medium and introduces magneto-Thomson and transverse Thomson coefficients. For the first time, we calculate the magneto-Thomson coefficient and transverse Thomson coefficient for the hot and dense hadron gas. The transverse Thomson effect originates due to the presence of the Nernst effect in the presence of a magnetic field [33]. In the absence of a magnetic field, the magneto-Thomson coefficient reduces to the Thomson coefficient, but the transverse Thomson coefficient vanishes completely.

To study the properties of the hot and dense hadronic medium created in the later stages of heavy-ion collisions, the ideal hadron resonance gas (IHRG) model has been widely used. It successfully describes thermodynamic quantities predicted by lattice QCD (lQCD) up to temperatures of approximately $T \approx 150$ MeV, beyond which hadron melting leads to notable deviations from lQCD [34, 35]. Unlike lQCD, which becomes computationally challenging at large baryon chemical potential due to the fermion sign problem [36, 37], the IHRG model remains useful for exploring hadronic matter at high baryon density. However, its inability to capture higher-order fluctuations of conserved charges, well-predicted by lQCD—has driven the development of improved models [38–40]. Among these, the excluded volume HRG (EVHRG) model introduces a finite size for hadrons, accounting for repulsive interactions via an excluded volume correction. This enhancement leads to better agreement with both thermodynamic observables and conserved charge fluctuations when compared to lQCD data [41–44]. Another model, the repulsive mean-field HRG (RMFHRG) model [45, 46], incorporates a mean-field potential to model inter-hadron repulsion. Recently, the van der Waals HRG (VDWHRG) model [47, 48] has gained attention for including both attractive and repulsive forces, making it one of the most realistic HRG extensions. It shows excellent agreement with lQCD predictions [48, 49] and also predicts a first-order liquid-gas phase transition at high baryon densities [50], offering valuable insights into dense nuclear matter.

In this work, we provide detailed calculations of the magneto-Thomson and transverse Thomson coefficients of the hot and dense hadronic medium in the presence of an external magnetic field. We use four different formalisms, namely, the IHRG, EVHRG, RMFHRG, and VDWHRG, to estimate the higher-order thermoelectric coefficients. This paper is organized in the following manner. Section (II) briefly introduces different HRG models, following which we present the derivation of both leading-order and higher-order thermoelectric coefficients in the presence of an external magnetic field. Section (III) discusses the results in detail, and finally, we summarize our study in Sec. (IV) with potential future directions.

II. FORMALISM

The current section highlights the calculations for both magneto-Thomson and transverse Thomson coefficients in the presence of an external magnetic field. Here, we solve the relativistic Boltzmann transport equation (RBTE) under relaxation time approximation (RTA). We discuss the hadron resonance gas model along with its extended versions that we use to calculate the higher-order thermoelectric coefficients of hot and dense hadron gas. Throughout the calculations, we have taken all the hadrons and their resonances up to the mass cut-off of

2.6 GeV from the particle data group [51].

A. Hadron resonance gas model

The Hadron Resonance Gas model is a theoretical framework used in high-energy nuclear physics to describe the thermodynamic properties of strongly interacting matter in the hadronic phase. The HRG model assumes that the hadronic matter is in thermal equilibrium, meaning that the temperature, chemical potential, and other thermodynamic variables are well-defined throughout the system. The various HRG models are discussed here.

1. Ideal hadron resonance gas model

The ideal HRG model consists of a system with volume V having non-interacting pointlike hadrons and resonances, for which the grand canonical partition function can be written as [52],

$$\ln Z_i^{id} = \pm \frac{V g_i}{2\pi^2} \int_0^\infty k_i^2 dk_i \ln\{1 \pm \exp[-(\omega_i - \mu_i)/T]\}. \quad (1)$$

Here, g_i is the degeneracy factor. The quantities k_i , m_i , and $\omega_i = \sqrt{k_i^2 + m_i^2}$ represents the momentum, mass, and energy of the i th hadron species, respectively. The \pm sign corresponds to fermions (upper) and bosons (lower). Considering a simplistic case of vanishing charge and strangeness chemical potential, the total chemical potential of the i th hadronic species, μ_i , is equal to the baryon chemical potential (μ_B) and is given by

$$\mu_i = \beta_i \mu_B, \quad (2)$$

where β_i denotes the baryon number of the i th hadron. The pressure P_i , energy density ε_i , and number density n_i can now be obtained from the partition function, given as,

$$P_i^{id}(T, \mu_i) = \pm \frac{T g_i}{2\pi^2} \int_0^\infty k_i^2 dk_i \ln\{1 \pm \exp[-(\omega_i - \mu_i)/T]\}, \quad (3)$$

$$\varepsilon_i^{id}(T, \mu_i) = \frac{g_i}{2\pi^2} \int_0^\infty \frac{\omega_i k_i^2 dk_i}{\exp[(\omega_i - \mu_i)/T] \pm 1}, \quad (4)$$

$$n_i^{id}(T, \mu_i) = \frac{g_i}{2\pi^2} \int_0^\infty \frac{k_i^2 dk_i}{\exp[(\omega_i - \mu_i)/T] \pm 1}. \quad (5)$$

2. Excluded volume hadron resonance gas model

The EVHRG model includes the repulsive interaction among the hadrons by considering a finite hardcore size of the hadrons. Therefore, the system volume (V) in the model is now replaced by the available volume (V_{avl}) that

mimics the short-range repulsive interaction among the hadrons.

$$V_{avl} = V - \sum_i N_i b_i, \quad (6)$$

where the N_i is number of i th hadron and $b_i (=16/3 \pi r_i^3)$ is the excluded volume. The r_i is the hardcore radius of each hadron. The pressure in the EVHRG model is then given by [53, 54]

$$P^{EV}(T, \mu) = P^{id}(T, \mu^*), \quad (7)$$

where $\mu^* = \mu - bP^{EV}(T, \mu)$ is an effective chemical potential. Other thermodynamic quantities can be readily obtained from Eq. (7) by taking appropriate derivatives. The number density and energy density, respectively, can be written as [53]

$$n^{EV}(T, \mu) = \sum_i \frac{n_i^{id}(T, \mu^*)}{1 + \sum_i b_i n_i^{id}(T, \mu^*)}, \quad (8)$$

$$\varepsilon^{EV}(T, \mu) = \sum_i \frac{\varepsilon_i^{id}(T, \mu^*)}{1 + \sum_i b_i n_i^{id}(T, \mu^*)}. \quad (9)$$

As we consider different hardcore radii for mesons and baryons, the repulsive parameter, b , contributes differently in the above-mentioned thermodynamic quantities.

3. van der Waals hadron resonance gas model

The VDWHRG model represents a real gas system by including attractive interactions among the hadrons along with repulsive interactions due to the excluded volume of the hadrons. With these interactions, the model predicts a liquid-gas phase transition which ends at a critical point [48]. In the hadronic models, these interactions are assumed to exist between all pairs of baryons and all pairs of antibaryons [47–49]. As in Ref. [13, 52], we also consider repulsive interactions among the mesons. The baryon-antibaryon and meson-(anti)baryon VDW interactions are neglected. The VDW equation of state in the canonical ensemble can be written as [49, 52]

$$P(T, n) = \frac{nT}{1 - bn} - an^2, \quad (10)$$

where a and b (positive) are the VDW parameters that describe attractive and repulsive interactions, respectively. P is the pressure of the system, whereas, $n = N/V$ is the number density. The repulsive interactions are included in the first term by replacing the total volume V with the effective volume available to particles using the proper volume parameter $b = 16\pi r^3/3$, as in the EVHRG model. The second term takes care of the attractive interactions between particles. The model reduces to EVHRG

when the attractive interaction parameter is set to zero, and further reduces to ideal HRG when both the attractive and repulsive interactions are neglected.

The VDW equation of state in the grand canonical ensemble can then be written as [49, 55]

$$P(T, \mu) = P^{id}(T, \mu^*) - an^2(T, \mu), \quad (11)$$

where the $n(T, \mu)$, the VDW particle number density can be written as

$$n(T, \mu) = \frac{\sum_i n_i^{id}(T, \mu_i^*)}{1 + b \sum_i n_i^{id}(T, \mu_i^*)}. \quad (12)$$

The μ^* is the modified chemical potential because of the interaction and is given by

$$\mu^* = \mu - bP(T, \mu) - abn^2(T, \mu) + 2an(T, \mu). \quad (13)$$

Because of the interaction among the hadrons, the contribution to total pressure in the VDWHRG model comes from the mesons, baryons, and antibaryons separately and is given by [48, 49]

$$P(T, \mu) = P_M(T, \mu) + P_B(T, \mu) + P_{\bar{B}}(T, \mu), \quad (14)$$

where the $P_M(T, \mu)$, $P_{B(\bar{B})}(T, \mu)$ are the pressures due to mesons and (anti)baryons, respectively and are given by,

$$P_M(T, \mu) = \sum_{i \in M} P_i^{id}(T, \mu^{*M}), \quad (15)$$

$$P_B(T, \mu) = \sum_{i \in B} P_i^{id}(T, \mu^{*B}) - an_B^2(T, \mu), \quad (16)$$

$$P_{\bar{B}}(T, \mu) = \sum_{i \in \bar{B}} P_i^{id}(T, \mu^{*\bar{B}}) - an_{\bar{B}}^2(T, \mu). \quad (17)$$

Here, M , B , and \bar{B} represent mesons, baryons, and antibaryons. Because of the excluded volume correction, the modified chemical potential for mesons is given by μ^{*M} , whereas, μ^{*B} and $\mu^{*\bar{B}}$ are the modified chemical potentials of baryons and antibaryons due to VDW interactions [56]. These modified chemical potentials for mesons and (anti)baryons can be obtained from Eq. (2) and Eq. (13) as,

$$\mu^{*M} = -b_M P_M(T, \mu), \quad (18)$$

$$\mu^{*B(\bar{B})} = \mu^{B(\bar{B})} - b_B P_{B(\bar{B})}(T, \mu) - ab_B n_{B(\bar{B})}^2 + 2an_{B(\bar{B})}, \quad (19)$$

where n_M , n_B and $n_{\bar{B}}$ are the modified number densities of mesons, baryons and antibaryons, respectively, which are given by

$$n_M(T, \mu) = \frac{\sum_{i \in M} n_i^{id}(T, \mu_i^{*M})}{1 + b_M \sum_{i \in M} n_i^{id}(T, \mu_i^{*M})}, \quad (20)$$

$$n_{B(\bar{B})}(T, \mu) = \frac{\sum_{i \in B(\bar{B})} n_i^{id}(T, \mu_i^{*B(\bar{B})})}{1 + b_B \sum_{i \in B(\bar{B})} n_i^{id}(T, \mu_i^{*B(\bar{B})})}. \quad (21)$$

The energy density for mesons and (anti)baryons can be obtained as,

$$\begin{aligned} \varepsilon(T, \mu)_M &= \frac{\sum_{i \in M} \varepsilon_i^{id}(T, \mu_i^*)}{1 + b_M \sum_{i \in M} n_i^{id}(T, \mu_i^*)}, \\ \varepsilon(T, \mu)_{B(\bar{B})} &= \frac{\sum_{i \in B(\bar{B})} \varepsilon_i^{id}(T, \mu_i^*)}{1 + b_B \sum_{i \in B(\bar{B})} n_i^{id}(T, \mu_i^*)} - an_{B(\bar{B})}^2(T, \mu). \end{aligned} \quad (22)$$

4. Repulsive mean-field hadron resonance gas model

In the RMFHRG model, the short-range repulsive interactions among the hadrons are taken into account in the mean field approach by considering a shift in the single-particle energies. This shift is proportional to the total number density of the hadrons. We use the repulsive mean field approach as in Ref. [45, 46, 57, 58] to include the repulsive interaction. The shift in the single-particle energy because of the interaction is given by

$$\tilde{\omega}_i = \sqrt{k_i^2 + m_i^2} + U(n) = \omega_i + U(n). \quad (23)$$

Here, U is the potential energy, which represents the repulsive interaction between hadrons and depends on the total hadron density n . For a given hadron potential $V(\mathbf{r})$, the potential energy can be expressed as $U(n) = Kn$. The phenomenological parameter K is determined by integrating the potential $V(\mathbf{r})$ over the spatial volume [45, 46].

In this work, we assign different repulsive interaction parameters for baryons and mesons. We denote the mean-field parameter for baryons (B) and antibaryons (\bar{B}) by K_B , while for mesons we denote it by K_M . Thus, for (anti)baryons

$$U(n_{B\{\bar{B}\}}) = K_B n_{B\{\bar{B}\}}, \quad (24)$$

and for mesons

$$U(n_M) = K_M n_M. \quad (25)$$

The repulsion parameter $K_B = 0.450 \text{ GeV fm}^3$ is taken to be the same for all (anti)baryons and $K_M = 0.050 \text{ GeV fm}^3$ for all mesons as in Ref. [59]. The total hadron number density is then given by

$$n(T, \mu) = \sum_i n_i = n_B + n_{\bar{B}} + n_M, \quad (26)$$

where n_i is the number density of i th hadronic species. Note that n_B , $n_{\bar{B}}$, and n_M are total baryon, antibaryon and meson number densities, respectively. Explicitly, for (anti)baryons,

$$n_{B\{\bar{B}\}} = \sum_{i \in B\{\bar{B}\}} \frac{g_i}{2\pi^2} \int_0^\infty \frac{k_i^2 dk_i}{e^{\left(\frac{\omega_i - \mu_i^{\text{eff}}}{T}\right)} + 1}. \quad (27)$$

Here, $\mu_{\text{eff}}^i = \beta_i \mu_B - U(n_{B\{\bar{B}\}})$ is the (anti)baryon effective chemical potential, with β_i being the baryonic number of i th baryon and μ_B , the baryon chemical potential. For mesons (since $\mu_B = 0$), the effective chemical potential becomes

$$(\mu_{\text{eff}}^i)_M = -U(n_M) = -K_M n_M. \quad (28)$$

Hence, the number density for mesons can be written as

$$n_M = \sum_{i \in M} \frac{g_i}{2\pi^2} \int_0^\infty \frac{k_i^2 dk_i}{e^{\left(\frac{\omega_i + K_M n_M}{T}\right)} - 1}, \quad (29)$$

where the sum is over all the mesons.

One can write the total (anti)baryon energy density as

$$\begin{aligned} \varepsilon_{B\{\bar{B}\}} &= \sum_{i \in B\{\bar{B}\}} \frac{g_i}{2\pi^2} \int_0^\infty \frac{k_i^2 dk_i \tilde{\omega}_i}{e^{\left(\frac{\omega_i - \mu_{\text{eff}}^i}{T}\right)} + 1} \\ &+ \phi_{B\{\bar{B}\}}(n_{B\{\bar{B}\}}), \end{aligned} \quad (30)$$

and for mesons

$$\varepsilon_M = \sum_{i \in M} \frac{g_i}{2\pi^2} \int_0^\infty \frac{k_i^2 dk_i \tilde{\omega}_i}{e^{\left(\frac{\omega_i + K_M n_M}{T}\right)} - 1} + \phi_M(n_M), \quad (31)$$

where $\phi(n)$ represents the energy density correction to avoid double-counting the potential. After doing the derivative of baryon energy density with respect to baryon net number density and using Eq. (24), we get

$$\frac{\partial \phi_{B\{\bar{B}\}}}{\partial n_{B\{\bar{B}\}}} = -K_B n_{B\{\bar{B}\}}, \quad (32)$$

and hence

$$\phi_B(n_{B\{\bar{B}\}}) = -\frac{1}{2} K_B n_{B\{\bar{B}\}}^2. \quad (33)$$

Also, for mesons, one can obtain in a similar way

$$\phi_M(n_M) = -\frac{1}{2} K_M n_M^2. \quad (34)$$

The pressure of the gas can now be readily obtained. For baryons

$$\begin{aligned} P_{B\{\bar{B}\}}(T, \mu) &= T \sum_{i \in B\{\bar{B}\}} \frac{g_i}{2\pi^2} \int_0^\infty k d_i^2 k_i \\ &\ln \left[1 + e^{-\left(\frac{\omega_i - \mu_{\text{eff}}^i}{T}\right)} \right] - \phi_{B\{\bar{B}\}}(n_{B\{\bar{B}\}}), \end{aligned} \quad (35)$$

and for mesons

$$\begin{aligned} P_M(T) &= -T \sum_{i \in M} \frac{g_i}{2\pi^2} \int_0^\infty k_i^2 dk_i \\ &\ln \left[1 - e^{-\left(\frac{\omega_i + K_M n_M}{T}\right)} \right] - \phi_M(n_M). \end{aligned} \quad (36)$$

B. Leading-order thermoelectric coefficients

To determine the leading-order thermoelectric coefficients in hot hadron gas, we begin with the relativistic Boltzmann transport equation under the relaxation time approximation. It provides a kinetic theory framework that tracks the phase-space distribution of particles, allowing one to model time-dependent processes like thermalization and transport. The presence of a magnetic field modifies the phase-space dynamics of charged particles through the Lorentz force, which introduces anisotropy in both electric and heat transport. Within RTA, the RBTE can be considered as a linear expansion of the single-particle total distribution function (f_i) around the single-particle equilibrium distribution function (f_i^0). Here, the total distribution function can be written as $f_i = f_i^0 + \delta f_i$, where δf_i is a non-equilibrium correction that represents the deviation from equilibrium. In the HRG model, each hadron species contributes to the total distribution function. For hadron species i with energy $\omega_i = \sqrt{k_i^2 + m_i^2}$, baryon number β_i , and the baryon chemical potential μ_B , the total single-particle distribution function is

$$f_i^0 = \frac{1}{e^{\frac{\omega_i - \beta_i \mu_B}{T}} \pm 1}, \quad (37)$$

where the \pm stands for fermion and boson, respectively. In local thermodynamic equilibrium, the spatial dependence of the distribution function appears due to spatial gradients of temperature and baryon chemical potential. The RBTE for a single hadron species under RTA in the presence of an electromagnetic field can be expressed as [4, 16]

$$k^\mu \partial_\mu f_i + q_i F^{\mu\nu} k_\nu \frac{\partial f_i}{\partial k^\mu} = -\frac{k^\mu u_\mu}{\tau_R^i} \delta f_i, \quad (38)$$

where $k^\mu = (\omega_i, \vec{k}_i)$ is the particle four-momentum, u^μ is the fluid four-velocity, $F^{\mu\nu}$ is the electromagnetic field tensor, and τ_R^i is the relaxation time for species i .

To solve the above equation, we take an ansatz to express the deviation of the distribution function from the equilibrium, such that it should reflect the driving forces. The general form of ansatz is [4, 5, 12, 60]

$$\delta f_i = \frac{\partial f_i^0}{\partial (k^\mu u_\mu)} k^\mu \Omega_\mu, \quad (39)$$

where the vector Ω^μ reflects the response of the distribution function to external thermodynamic forces such as temperature gradients, electric fields, and magnetic fields. In the fluid rest frame ($u^\mu = (1, \vec{0})$), Ω^μ can be decomposed as

$$\begin{aligned} \Omega^\mu &= \alpha_1 E^\mu + \alpha_2 B^\mu + \alpha_3 \epsilon^{\mu\nu\rho\sigma} u_\nu E_\rho B_\sigma + \alpha_4 \nabla^\mu T \\ &+ \alpha_5 \epsilon^{\mu\nu\rho\sigma} u_\nu \nabla_\rho T B_\sigma + \alpha_6 \epsilon^{\mu\nu\rho\sigma} u_\nu \nabla_\rho T E_\sigma, \end{aligned} \quad (40)$$

where the electric and magnetic fields in the fluid rest frame are

$$E^\mu = F^{\mu\nu}u_\nu, \quad B^\mu = \frac{1}{2}\epsilon^{\mu\nu\rho\sigma}u_\nu F_{\rho\sigma},$$

and $\nabla^\mu = \Delta^{\mu\nu}\partial_\nu$ is the spatial gradient orthogonal to u^μ , with $\Delta^{\mu\nu} = g^{\mu\nu} - u^\mu u^\nu$. Here, ϵ^{ijkl} denotes the Levi-Civita symbol, which is used to represent antisymmetric tensor components.

Using Eq.(39) into RBTE as given in Eq.(38) and projecting onto spatial components in the local rest frame yields [13],

$$\begin{aligned} & \vec{v}_i \cdot \left[-\frac{\partial f_i^0}{\partial \omega_i} \left(\frac{\omega_i - \beta_i h}{T} \right) \vec{\nabla} T \right] + q_i (\vec{E} \cdot \vec{v}_i) \frac{\partial f_i^0}{\partial \omega_i} \\ & - q_i \vec{v}_i \cdot (\vec{\Omega} \times \vec{B}) \frac{\partial f_i^0}{\partial \omega_i} = -\frac{\omega_i}{\tau_R^i} (\vec{v}_i \cdot \vec{\Omega}) \frac{\partial f_i^0}{\partial \omega_i}. \end{aligned} \quad (41)$$

Where $\vec{v}_i = \vec{k}_i/\omega_i$ is the relativistic particle velocity. By substituting $\vec{\Omega}$ from Eq.(40) into Eq.(41), we can expand it analogously to the nonrelativistic case as,

$$\begin{aligned} & q_i (\vec{E} \cdot \vec{v}_i) - \alpha_1 q_i \vec{v}_i \cdot (\vec{E} \times \vec{B}) - \alpha_3 q_i (\vec{E} \cdot \vec{B}) (\vec{v}_i \cdot \vec{B}) + \alpha_3 \\ & q_i (\vec{v}_i \cdot \vec{E}) - \alpha_4 q_i \vec{v}_i \cdot (\vec{\nabla} T \times \vec{B}) - \alpha_5 q_i (\vec{\nabla} T \cdot \vec{B}) (\vec{v}_i \cdot \vec{B}) \\ & + \alpha_5 q_i (\vec{v}_i \cdot \vec{\nabla} T) - \alpha_6 q_i (\vec{\nabla} T \cdot \vec{B}) (\vec{v}_i \cdot \vec{E}) + \alpha_6 q_i (\vec{E} \cdot \vec{B}) (\vec{v}_i \cdot \vec{\nabla} T) \\ & - \left(\frac{\omega_i - \beta_i h}{T} \right) (\vec{v}_i \cdot \vec{\nabla} T) = -\frac{\omega_i}{\tau_R^i} \left[\alpha_1 (\vec{v}_i \cdot \vec{E}) + \alpha_2 (\vec{v}_i \cdot \vec{B}) \right. \\ & + \alpha_3 \vec{v}_i \cdot (\vec{E} \times \vec{B}) + \alpha_4 (\vec{v}_i \cdot \vec{\nabla} T) + \alpha_5 \vec{v}_i \cdot (\vec{\nabla} T \times \vec{B}) + \\ & \left. \alpha_6 \vec{v}_i \cdot (\vec{\nabla} T \times \vec{E}) \right]. \end{aligned} \quad (42)$$

Comparing the coefficients of same tensor structures on both sides of Eq.(42) we get,

$$\alpha_1 = -\frac{\tau_R^i}{\omega_i} (q_i E + \alpha_3 q_i B), \quad (43)$$

$$\alpha_2 = \alpha_3 \tau_R^i \Omega_{c_i} (\vec{E} \cdot \vec{B}) + b \tau_R^i \Omega_{c_i} (\vec{\nabla} T \cdot \vec{B}), \quad (44)$$

$$\alpha_3 = \alpha_1 \tau_R^i \Omega_{c_i}, \quad (45)$$

$$\alpha_4 = \frac{\tau_R^i}{\omega_i} \left(\frac{\omega_i - \beta_i h}{T} \right) - \alpha_5 \tau_R^i \Omega_{c_i}, \quad (46)$$

$$\alpha_5 = \Omega_{c_i} \tau_R^i \alpha_4, \quad (47)$$

$$\alpha_6 = 0. \quad (48)$$

where $\Omega_{c_i} = \frac{q_i B}{\omega_i}$ represents the cyclotron frequency of the particle with electric charge q_i . Using Eqs.(43) to (48), we get

$$\alpha_1 = -\frac{(q_i E) (\tau_R^i / \omega_i)}{1 + (\Omega_{c_i} \tau_R^i)^2}, \quad (49)$$

$$\alpha_4 = \frac{\tau_R^i}{\omega_i} \left(\frac{\omega_i - \beta_i h}{T} \right) \frac{1}{1 + (\Omega_{c_i} \tau_R^i)^2}. \quad (50)$$

Using α_1 and α_4 as given in Eq.(49) and Eq.(50), we can write deviation from the equilibrium distribution function as,

$$\begin{aligned} \delta f_i = & \frac{\tau_R^i}{1 + (\Omega_{c_i} \tau_R^i)^2} \left[q_i \left\{ (\vec{v}_i \cdot \vec{E}) + (\Omega_{c_i} \tau_R^i) \vec{v}_i \cdot (\vec{E} \times \vec{B}) + \right. \right. \\ & \left. \left. (\Omega_{c_i} \tau_R^i)^2 (\vec{E} \cdot \vec{B}) (\vec{v}_i \cdot \vec{B}) \right\} - \left(\frac{\omega_i - \beta_i h}{T} \right) \left\{ (\vec{v}_i \cdot \vec{\nabla} T) + \right. \right. \\ & \left. \left. (\Omega_{c_i} \tau_R^i) \vec{v}_i \cdot (\vec{\nabla} T \times \vec{B}) + (\Omega_{c_i} \tau_R^i)^2 (\vec{\nabla} T \cdot \vec{B}) (\vec{v}_i \cdot \vec{B}) \right\} \right] \left(-\frac{\partial f_i^0}{\partial \omega_i} \right). \end{aligned} \quad (51)$$

Now, we can express the electrical current and the heat current using δf_i as given in Eq.(51) as,

$$\begin{aligned} j^l = & \sum_i g_i \int \frac{d^3 k_i}{(2\pi)^3} q_i v_i^l \delta f_i \\ = & \sum_i \frac{g_i q_i}{3} \int \frac{d^3 k_i}{(2\pi)^3} \frac{v_i^2 \tau_R^i}{1 + (\Omega_{c_i} \tau_R^i)^2} \left[q_i \delta^{lj} E^j + q_i (\Omega_{c_i} \tau_R^i) \right. \\ & \left. \epsilon^{ljk} h^k E^j + q_i (\Omega_{c_i} \tau_R^i)^2 h^l h^j E^j - \left(\frac{\omega_i - \beta_i h}{T} \right) \left\{ \delta^{lj} \frac{\partial T}{\partial x^j} \right. \right. \\ & \left. \left. + (\Omega_{c_i} \tau_R^i) \epsilon^{ljk} h^k \frac{\partial T}{\partial x^j} + (\Omega_{c_i} \tau_R^i)^2 h^l h^j \frac{\partial T}{\partial x^j} \right\} \right] \left(-\frac{\partial f_i^0}{\partial \omega_i} \right), \end{aligned} \quad (52)$$

and,

$$\begin{aligned} I^l = & \sum_i g_i \int \frac{d^3 k_i}{(2\pi)^3} v_i^l (\omega_i - \beta_i h) \delta f_i \\ = & \sum_i \frac{g_i}{3} \int \frac{d^3 k_i}{(2\pi)^3} \frac{v_i^2 \tau_R^i}{1 + (\Omega_{c_i} \tau_R^i)^2} (\omega_i - \beta_i h) \left[q_i \delta^{lj} E^j \right. \\ & \left. + q_i (\Omega_{c_i} \tau_R^i) \epsilon^{ljk} h^k E^j + q_i (\Omega_{c_i} \tau_R^i)^2 h^l h^j E^j - \left(\frac{\omega_i - \beta_i h}{T} \right) \right. \\ & \left. \left\{ \delta^{lj} \frac{\partial T}{\partial x^j} + (\Omega_{c_i} \tau_R^i) \epsilon^{ljk} h^k \frac{\partial T}{\partial x^j} + (\Omega_{c_i} \tau_R^i)^2 h^l h^j \frac{\partial T}{\partial x^j} \right\} \right] \\ & \left(-\frac{\partial f_i^0}{\partial \omega_i} \right). \end{aligned} \quad (53)$$

Here, to simplify further calculations, we can choose the magnetic field along the z direction. The direction of the electric field and the temperature gradient are perpendicular to the z axis, i.e., it is in the $x - y$ plane. Under these conditions, the components of the electric current in the $x - y$ plane are given as,

$$\begin{aligned} j_x = & \sum_i \frac{g_i q_i}{3} \int \frac{d^3 k_i}{(2\pi)^3} \frac{v_i^2 q_i \tau_R^i}{1 + (\Omega_{c_i} \tau_R^i)^2} \left[E_x + (\Omega_{c_i} \tau_R^i) E_y \right] \\ & \left(-\frac{\partial f_i^0}{\partial \omega_i} \right) - \sum_i \frac{g_i q_i}{3T} \int \frac{d^3 k_i}{(2\pi)^3} \frac{v_i^2 \tau_R^i (\omega_i - \beta_i h)}{1 + (\Omega_{c_i} \tau)^2} \\ & \left[\frac{dT}{dx} + (\Omega_{c_i} \tau_R^i) \frac{dT}{dy} \right] \left(-\frac{\partial f_i^0}{\partial \omega_i} \right), \end{aligned} \quad (54)$$

and,

$$\begin{aligned}
j_y &= \sum_i \frac{g_i q_i}{3} \int \frac{d^3 k_i}{(2\pi)^3} \frac{v_i^2 q_i \tau_R^i}{1 + (\Omega_{c_i} \tau_R^i)^2} \left[E_y - (\Omega_{c_i} \tau_R^i) E_x \right] \\
&(-) \frac{\partial f_i^0}{\partial \omega_i} - \sum_i \frac{g_i q_i}{3T} \int \frac{d^3 k_i}{(2\pi)^3} \frac{v_i^2 \tau_R^i (\omega_i - \beta_i \hbar)}{1 + (\Omega_{c_i} \tau)^2} \\
&\left[\frac{dT}{dy} - (\Omega_{c_i} \tau_R^i) \frac{dT}{dx} \right] \left(-\frac{\partial f_i^0}{\partial \omega_i} \right). \quad (55)
\end{aligned}$$

Eqs.(54) and (55) can be written in a compact form by introducing the following integrals,

$$H_{1_i} = \frac{g_i}{3} \int \frac{d^3 k_i}{(2\pi)^3} \frac{\tau_R^i}{1 + (\Omega_{c_i} \tau_R^i)^2} \left(\frac{\vec{k}_i}{\omega_i^2} \right) \left(-\frac{\partial f_i^0}{\partial \omega_i} \right), \quad (56)$$

$$H_{2_i} = \frac{g_i}{3} \int \frac{d^3 k_i}{(2\pi)^3} \frac{\tau_R^i (\Omega_{c_i} \tau_R^i)}{1 + (\Omega_{c_i} \tau_R^i)^2} \left(\frac{\vec{k}_i}{\omega_i^2} \right) \left(-\frac{\partial f_i^0}{\partial \omega_i} \right), \quad (57)$$

$$H_{3_i} = \frac{g_i}{3} \int \frac{d^3 k_i}{(2\pi)^3} \frac{\tau_R^i \omega_i}{1 + (\Omega_{c_i} \tau_R^i)^2} \left(\frac{\vec{k}_i}{\omega_i^2} \right) \left(-\frac{\partial f_i^0}{\partial \omega_i} \right), \quad (58)$$

$$H_{4_i} = \frac{g_i}{3} \int \frac{d^3 k_i}{(2\pi)^3} \frac{\tau_R^i \omega_i (\Omega_{c_i} \tau_R^i)}{1 + (\Omega_{c_i} \tau_R^i)^2} \left(\frac{\vec{k}_i}{\omega_i^2} \right) \left(-\frac{\partial f_i^0}{\partial \omega_i} \right). \quad (59)$$

$$j_x = \sum_i q_i^2 H_{1_i} E_x + \sum_i q_i^2 H_{2_i} E_y - \frac{1}{T} \sum_a q_i \left(H_{3_i} - \beta_i \hbar H_{1_i} \right) \frac{dT}{dx} - \frac{1}{T} \sum_a q_i \left(H_{4_i} - \beta_i \hbar H_{2_i} \right) \frac{dT}{dy}, \quad (60)$$

and,

$$j_y = \sum_i q_i^2 H_{1_i} E_y - \sum_i q_i^2 H_{2_i} E_x - \frac{1}{T} \sum_a q_i \left(H_{3_i} - \beta_i \hbar H_{1_i} \right) \frac{dT}{dy} + \frac{1}{T} \sum_a q_i \left(H_{4_i} - \beta_i \hbar H_{2_i} \right) \frac{dT}{dx}. \quad (61)$$

Here, in the presence of a magnetic field, the magneto-Seebeck coefficient (S_B) can be determined by setting $j_x = j_y = 0$ so that the electric field becomes proportional to the temperature gradient. For $j_x = 0$ and $j_y = 0$ we can solve Eqs.(60) and (61) to get E_x and E_y in terms of temperature gradients $\frac{dT}{dx}$ and $\frac{dT}{dy}$ as,

$$\begin{aligned}
E_x &= \frac{\sum_i q_i^2 H_{1_i} \sum_i q_i (H_{3_i} - \beta_i \hbar H_{1_i}) + \sum_i q_i^2 H_{2_i} \sum_i q_i (H_{4_i} - \beta_i \hbar H_{2_i})}{T \left[\left(\sum_i q_i^2 H_{1_i} \right)^2 + \left(\sum_i q_i^2 H_{2_i} \right)^2 \right]} \frac{dT}{dx} \\
&+ \frac{\sum_i q_i^2 H_{1_i} \sum_i q_i (H_{4_i} - \beta_i \hbar H_{2_i}) - \sum_i q_i^2 H_{2_i} \sum_i q_i (H_{3_i} - \beta_i \hbar H_{1_i})}{T \left[\left(\sum_i q_i^2 H_{1_i} \right)^2 + \left(\sum_i q_i^2 H_{2_i} \right)^2 \right]} \frac{dT}{dy}, \quad (62)
\end{aligned}$$

and,

$$\begin{aligned}
E_y &= \frac{\sum_i q_i^2 H_{2_i} \sum_i q_i (H_{3_i} - \beta_i \hbar H_{1_i}) - \sum_i q_i^2 H_{1_i} \sum_i q_i (H_{4_i} - \beta_i \hbar H_{2_i})}{T \left[\left(\sum_i q_i^2 H_{1_i} \right)^2 + \left(\sum_i q_i^2 H_{2_i} \right)^2 \right]} \frac{dT}{dx} \\
&+ \frac{\sum_i q_i^2 H_{1_i} \sum_i q_i (H_{3_i} - \beta_i \hbar H_{1_i}) + \sum_i q_i^2 H_{2_i} \sum_i q_i (H_{4_i} - \beta_i \hbar H_{2_i})}{T \left[\left(\sum_i q_i^2 H_{1_i} \right)^2 + \left(\sum_i q_i^2 H_{2_i} \right)^2 \right]} \frac{dT}{dy}. \quad (63)
\end{aligned}$$

Eqs.(62) and (63) can be written in a compact form in

The integrals as given in Eqs.(56)-(59) allows us to write Eq.(54) and Eq.(55), respectively, as

the following way,

$$\begin{pmatrix} E_x \\ E_y \end{pmatrix} = \begin{pmatrix} S_B & NB \\ -NB & S_B \end{pmatrix} \begin{pmatrix} \frac{dT}{dx} \\ \frac{dT}{dy} \end{pmatrix}, \quad (64)$$

here one can identify the magneto-Seebeck coefficient as,

$$S_B = \frac{\sum_i q_i^2 H_{1i} \sum_i q_i (H_{3i} - \beta_i h H_{1i}) + \sum_i q_i^2 H_{2i} \sum_i q_i (H_{4i} - \beta_i h H_{2i})}{T \left[\left(\sum_i q_i^2 H_{1i} \right)^2 + \left(\sum_i q_i^2 H_{2i} \right)^2 \right]} = \frac{(\sigma_{el}/T)(\mathcal{I}_{31}/T^2) + (\sigma_H/T)(\mathcal{I}_{42}/T^2)}{(\sigma_{el}/T)^2 + (\sigma_H/T)^2}, \quad (65)$$

and the normalized Nernst coefficient (NB) is given as,

$$NB = \frac{\sum_i q_i^2 H_{1i} \sum_i q_i (H_{4i} - \beta_i h H_{2i}) - \sum_i q_i^2 H_{2i} \sum_i q_i (H_{3i} - \beta_i h H_{1i})}{T \left[\left(\sum_i q_i^2 H_{1i} \right)^2 + \left(\sum_i q_i^2 H_{2i} \right)^2 \right]} = \frac{(\sigma_{el}/T)(\mathcal{I}_{42}/T^2) - (\sigma_H/T)(\mathcal{I}_{31}/T^2)}{(\sigma_{el}/T)^2 + (\sigma_H/T)^2}. \quad (66)$$

Here, we have identified the ohmic-like component of electrical conductivity in the presence of a magnetic field and the Hall-like component of electrical conductivity as $\sigma_{el} = \sum_i q_i^2 H_{1i}$ and $\sigma_H = \sum_i q_i^2 H_{2i}$ respectively [12]. The integrals \mathcal{I}_{31} and \mathcal{I}_{42} in Eqs.(65) and (66) are defined as $\mathcal{I}_{31} = \sum_i q_i (H_{3i} - \beta_i h H_{1i})$ and $\mathcal{I}_{42} = \sum_i q_i (H_{4i} - \beta_i h H_{2i})$. Note that in the absence of a magnetic field, integrals H_{2i} and H_{4i} are identically zero. Hence, the normalized Nernst coefficient vanishes in the absence of a magnetic field, and the magneto-Seebeck coefficient reduces to the Seebeck coefficient in the absence of a magnetic field [13]. The coefficients S_B and NB have temperature dependence as shown in Eqs. 65 and 66, hence the higher-order thermoelectric coefficients are introduced for the medium.

C. Higher-order thermoelectric coefficients

Higher-order thermoelectric coefficients differ from their leading-order counterparts in behavior. While leading-order effects such as the Seebeck or Peltier effects arise from linear responses to small gradients in temperature or electric field, higher-order phenomena manifest when systems are subjected to non-linear responses. The temperature dependence of the leading-order thermoelectric coefficient, such as the Seebeck coefficient, further gives rise to the higher-order thermoelectric coefficients. The presence of the leading-order thermoelectric coefficient in the conducting medium modifies the charge current and heat current of the medium as [13, 16]

$$\begin{aligned} \vec{j} &= \sigma_{el} \vec{E} - \sigma_{el} S \vec{\nabla} T, \\ \vec{I} &= T \sigma_{el} S \vec{E} - \kappa_0 \vec{\nabla} T, \end{aligned} \quad (67)$$

where κ_0 is the thermal conductivity of the medium and is expressed as [13]

$$\kappa_0 = \sum_i \frac{g_i}{3T^2} \int \frac{d^3 k_i}{(2\pi)^3} \tau_R^i \left(\frac{\vec{k}_i}{\omega_i} \right)^2 (\omega_i - \beta_i h)^2 f_i^0 (1 \mp f_i^0). \quad (68)$$

Using Eq.(67), we can express the heat current \vec{I} in terms of electric current \vec{j} in the following way,

$$\vec{I} = T S \vec{j} - (\kappa_0 - T \sigma_{el} S^2) \vec{\nabla} T. \quad (69)$$

Here, $\kappa' = \kappa_0 - T \sigma_{el} S^2$ is defined as the modified thermal conductivity of the medium. The Eq.(67) can be defined in matrix form as

$$\begin{pmatrix} \vec{j} \\ \vec{I} \end{pmatrix} = \begin{pmatrix} \sigma_{el} & \sigma_{el} S T \\ \sigma_{el} S T & \kappa_0 T \end{pmatrix} \begin{pmatrix} \vec{E} \\ -\vec{\nabla} T / T \end{pmatrix}. \quad (70)$$

The above matrix can be rearranged and expressed as follows

$$\begin{pmatrix} \vec{E} \\ \vec{I} \end{pmatrix} = \begin{pmatrix} \rho_{el} & S \\ S T & -\kappa' \end{pmatrix} \begin{pmatrix} \vec{j} \\ -\vec{\nabla} T / T \end{pmatrix}, \quad (71)$$

where resistivity of the medium is $\rho_{el} = 1/\sigma_{el}$. When a magnetic field is introduced in the z direction, electric field and temperature gradients in x-y plane, the above matrix in x-y plane can be expressed as

$$\begin{pmatrix} E_x \\ E_y \\ I_x \\ I_y \end{pmatrix} = \begin{pmatrix} \rho_{el} & \rho_H & S_B & NB \\ -\rho_H & \rho_{el} & -NB & S_B \\ S_B T & NB T & -\kappa'_{el} & -\kappa'_H \\ -NB T & S_B T & \kappa'_H & -\kappa'_{el} \end{pmatrix} \begin{pmatrix} j_x \\ j_y \\ \frac{dT}{dx} \\ \frac{dT}{dy} \end{pmatrix}, \quad (72)$$

The κ_{el} and κ_H are Ohmic-like and Hall-like components of thermal conductivity of the medium in the presence of a magnetic field [5], such that $\kappa'_{el} = \kappa_{el} - T\sigma_{el}S_B^2$ and $\kappa'_H = \kappa_H - T\sigma_H(NB)^2$. Also the $\rho_H = 1/\sigma_H$.

For any conducting medium having non-zero current density and temperature gradients along the x direction and an applied magnetic field along the z direction, the heat production rate per unit volume (\dot{Q}) can be expressed as [33]

$$\begin{aligned}\dot{Q} &= E_x j_x - \frac{dI_x}{dx} \\ &= (\rho_{el} j_x + S_B \frac{dT}{dx}) j_x - \frac{dT}{dx} (S_B T j_x - \kappa'_{el} \frac{dT}{dx}) \\ &= \rho_{el} j_x^2 + \frac{dT}{dx} (\kappa'_{el} \frac{dT}{dx}) - (T \frac{dS_B}{dT}) j_x \frac{dT}{dx}.\end{aligned}\quad (73)$$

The last term in the above equation is the heat generated by the combined action of j_x and $\frac{dT}{dx}$. The heat production rate per unit volume due to the Thomson effect in the presence of a magnetic field is given by [61]

$$\dot{Q} = -Th_B (\vec{j} \cdot \vec{\nabla} T) \quad (74)$$

Finally, from Eqs. 76 and 74 we can define the magneto-Thomson coefficient (Th_B) as

$$Th_B = T \frac{dS_B}{dT}. \quad (75)$$

In the absence of a magnetic field, the coefficient Th_B reduces to the Thomson coefficient Th [13, 62].

The transverse Thomson coefficient (Th_N) is introduced in the medium because of the presence of a finite value of the normalized Nernst coefficient. In general, the coefficient Th_N is expected to occur when a charge current, temperature gradient, and magnetic field are oriented perpendicular to each other in any conducting medium. We consider the heat production rate per unit volume when the current density is along the x direction and temperature gradients are along the y direction, whereas a magnetic field is directed along the z axis. Hence, the heat production rate per unit volume is

$$\begin{aligned}\dot{Q} &= E_x j_x - \frac{dI_y}{dy} \\ &= (\rho_{el} j_x + NB \frac{dT}{dy}) j_x - \frac{dT}{dy} (-NB T j_x - \kappa'_{el} \frac{dT}{dy}) \\ &= \rho_{el} j_x^2 + \frac{dT}{dy} (\kappa'_{el} \frac{dT}{dy}) + (T \frac{d(NB)}{dT} + 2NB) j_x \frac{dT}{dy}.\end{aligned}\quad (76)$$

Therefore, the transverse Thomson coefficient is defined as

$$Th_N = T \frac{d(NB)}{dT} + 2NB. \quad (77)$$

Unlike the Th_B , the coefficient Th_N not only depends on the temperature derivative of the leading thermoelectric coefficient (for this case NB) but also on its magnitude [33]. In the absence of a magnetic field, the coefficient Th_N vanishes because of the vanishing NB .

In the above calculation, for the sake of simplicity, we take the thermal averaged relaxation time after integrating the energy-dependent relaxation time over the equilibrium distribution function. The thermal averaged relaxation time (τ_R^i) for the i th hadron species can be expressed in terms of scattering cross-section as [16],

$$\tau_R^{i-1} = \sum_j n_j \langle \sigma_{ij} v_{ij} \rangle \quad (78)$$

where,

$$\begin{aligned}\langle \sigma_{ij} v_{ij} \rangle &= \frac{\sigma}{8T m_i^2 m_j^2 \mathcal{K}_2(m_i/T) \mathcal{K}_2(m_j/T)} \times \\ &\int_{(m_i+m_j)^2}^{\infty} ds \times \\ &\frac{[s - (m_i - m_j)^2]}{\sqrt{s}} \times [s - (m_i + m_j)^2] \mathcal{K}_1(\sqrt{s}/T),\end{aligned}\quad (79)$$

Here, $\sigma = 4\pi r_h^2$ is the total scattering cross-section for the hard spheres, and it is independent of both temperature and baryon chemical potential. $\mathcal{K}_1, \mathcal{K}_2$ are modified Bessel functions of the first and second order.

III. RESULTS AND DISCUSSIONS

In this section, we discuss the results for higher-order thermoelectric coefficients of a hot and dense hadron gas in the presence of an external magnetic field. We also present a short description of the Thomson coefficient to show a comparative analysis between the magneto-Thomson coefficient and the Thomson coefficient. While the latter was estimated from the analysis of the Seebeck coefficient in our previous study [13], the results shown here are obtained from more complete and rigorous calculations. This allows for a qualitative understanding of how the presence of a magnetic field modifies the higher-order transport properties, particularly in relation to the temperature dependence and baryon chemical potential. We have considered four different versions of hadron resonance gas models, including a discrete particle spectrum having all the hadrons and their resonances up to the mass cutoff $\Lambda = 2.6$ GeV [51]. To estimate the relaxation time of the hadrons, we follow the hard-scattering approximation. A uniform radius, $r_m = 0.2$ fm for mesons and $r_{b,\bar{b}} = 0.62$ fm for baryons and antibaryons throughout the calculations [52]. For the VDWHRG model, we take van der Waals parameters as $a = 0.926$ GeV fm³ and $b = (16/3)\pi r^3$ [49, 52].

Fig. 1 represents the Thomson coefficient Th as a function of temperature T for three different baryon chemical potentials, i.e., at $\mu_B = 0.10, 0.30,$ and 0.40 GeV. The black solid line represents the Thomson coefficient obtained in the IHRG model, whereas the red dotted line represents the EVHRG model. The green and cyan dashed lines represent the same for the RMFHRG and

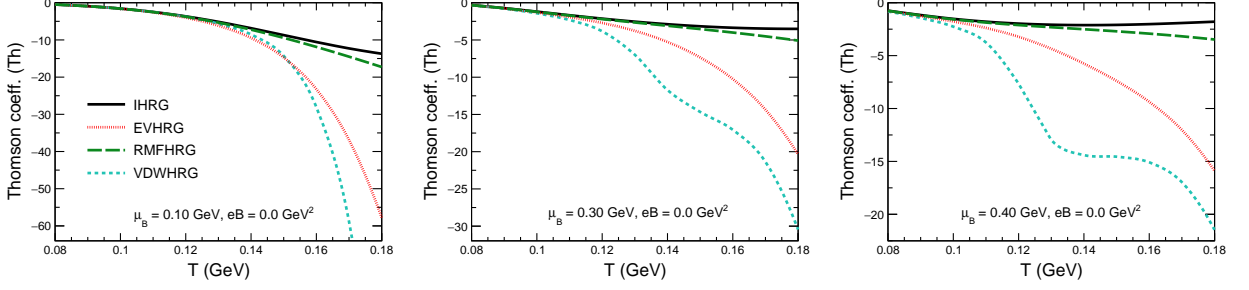


FIG. 1: Thomson coefficient (Th) obtained in different hadronic models as a function of temperature at $\mu_B = 0.10$ GeV (left panel), 0.30 GeV (middle panel), and 0.40 GeV (right panel).

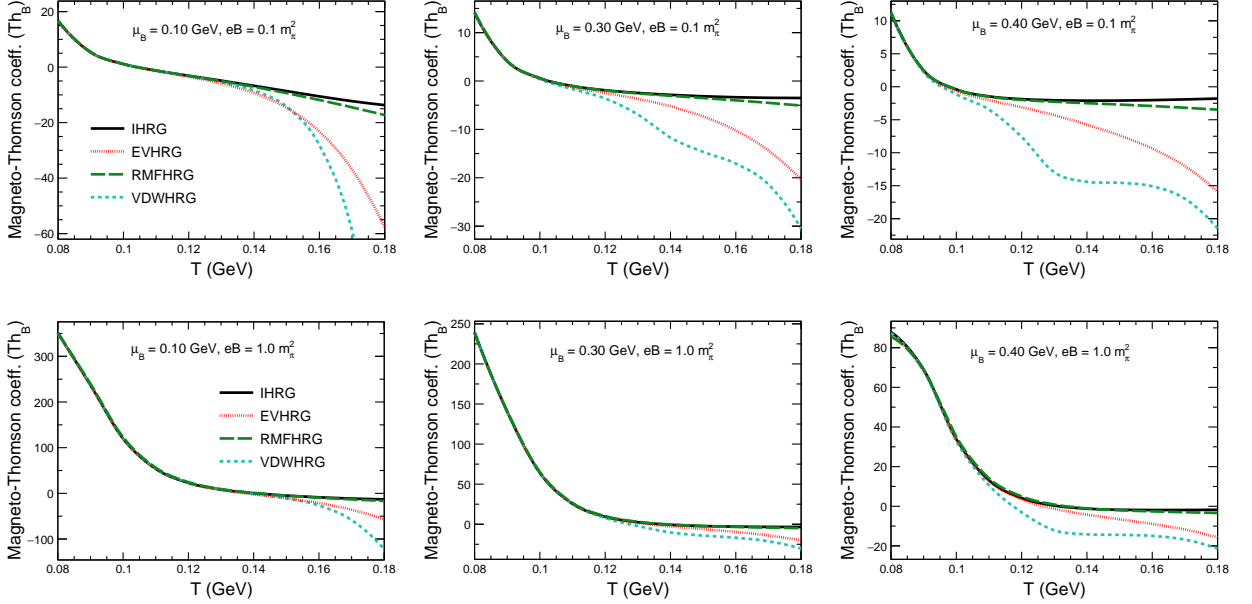


FIG. 2: Magneto-Thomson coefficient (Th_B) as a function of temperature at magnetic field $eB = 0.1 m_\pi^2$ (upper panel) and $eB = 1.0 m_\pi^2$ (lower panel) for baryon chemical potential at $\mu_B = 0.10$ GeV (left), 0.30 GeV (middle), and 0.40 GeV (right).

VDWHRG models, respectively. It is observed that for the chosen range of temperature ($0.08 - 0.18$ GeV), Th is negative for a hot and dense hadron gas. The Th is universally decreasing as the temperature increases. However, the degree of decrease is different for different models. To define the net heat flow for a relativistic system, we need a conserved charge. For the study of the HRG system, the heat current corresponds to the net baryon current. It is observed that the baryons have a dominant contribution over the mesons to the Thomson coefficient. The mesons contribute to thermoelectricity only through the enthalpy of the system. In hadron gas, the entropy production for lighter mesons like pions, kaons, etc., is higher. Therefore, the enthalpy per baryon (h) exceeds the single-particle energy (ω_i), which results in the negative values of Th [13]. The positive (negative) values of the Thomson coefficient lead to the net

absorption (release) of heat in the system. Therefore, a non-zero Thomson coefficient can significantly affect the cooling dynamics of the medium. The Thomson coefficient can be calculated as the product of temperature and the rate of change of the Seebeck coefficient with respect to temperature [13]; therefore, the higher the rate of change of the Seebeck coefficient with temperature, the higher the value of Th in magnitude as a function of T . The coefficient Th shows overlap at lower values of temperature nearly up to ≈ 0.14 GeV for the case of $\mu_B = 0.10$ GeV. As the value of μ_B increases, the models start deviating from each other even at low temperatures. Additionally, a noticeable flatness appears in the VDWHRG model in the temperature range around $T \approx 0.13-0.16$ GeV for $\mu_B = 0.40$ GeV, indicating a plateau-like behavior of the Thomson coefficient in this region. On the other hand, the constant decreasing rate of the

Seebeck coefficient around the above-mentioned temperature range [13] leads to the constant slope. Hence, the Th shows a non-monotonic behavior at high values of μ_B .

The upper panel of Fig. 2 represents Th_B as a function of T for three different values of μ_B at 0.10, 0.30, and 0.40 GeV at magnetic field $0.1 m_\pi^2$, whereas the lower panel represents those for the magnetic field $1.0 m_\pi^2$. For the case of $eB = 0.1 m_\pi^2$, we observe that Th_B decreases with the temperature up to 0.1 GeV, becomes zero at a particular T , and further, it starts to increase in the negative direction for higher values of temperature. Similar to what was observed in the case of a vanishing magnetic field, all the models agree up to a certain temperature and then start deviating from each other at higher temperatures. Furthermore, we also observe that the values of Th_B increase in the negative direction with the increasing values of μ_B for higher T but decrease in the positive direction for the lower values of T . Unlike the case without a magnetic field, the magneto-Thomson coefficient Th_B exhibits an additional dependence on the Hall-like component of electrical conductivity and other integral terms that arise due to the presence of an external magnetic field. The Hall-like conductivity term, σ_H/T , increases with baryon chemical potential μ_B because of the growing net baryonic contributions. It is important to note that mesons do not contribute directly to the integrals \mathcal{I}_{31}/T^2 and \mathcal{I}_{42}/T^2 , though their influence appears indirectly through the enthalpy per baryon h . The effect of the magnetic field is significant on \mathcal{I}_{31}/T^2 at low temperatures, but almost diminishes at higher temperatures due to a reduced relaxation time. On the other hand, \mathcal{I}_{42}/T^2 first increases with temperature and then starts to decrease. The higher the magnetic field, the lower the \mathcal{I}_{42}/T^2 . Here, the magnitude of σ_{el}/T is significantly larger than that of σ_H/T , the integrals \mathcal{I}_{31}/T^2 and \mathcal{I}_{42}/T^2 are of comparable scale [63]. Consequently, the magneto-Seebeck coefficient S_B can be approximately represented by the ratio $(\mathcal{I}_{31}/T^2)/(\sigma_{el}/T)$, and its temperature dependence is reflected in the behavior of the magneto-Thomson coefficient Th_B , as shown in Fig. 2. The T and μ_B dependence of σ_{el}/T in a magnetic field causes S_B to increase at low T and decrease at high T . This results in a positive Th_B at lower temperatures, which decreases with T and becomes negative at higher temperatures. At low T , a large value of $\Omega_{c_i} \tau_{R_i}$ suppresses the mesonic contribution to σ_{el}/T , and this reduction is compensated by the enhanced baryonic contribution as μ_B increases. However, at higher temperatures, the baryonic increase is insufficient to compensate for the mesonic suppression, leading to an overall decrease in σ_{el}/T with μ_B . For stronger magnetic fields, as shown in the lower panel of Fig. 2, Th_B shows large and positive values at low T , gradually approaching zero at high T . It is observed that for higher values of a magnetic field, results from all the models agree up to $T \approx 0.15$ GeV at $\mu_B = 0.10$ GeV. With increasing values of μ_B , the disagreement between the models starts from even lower

values of T . This observation is in line with what was observed for the magneto-Seebeck coefficient in Ref. [13].

In the presence of an external magnetic field, we also observe a Hall-like component for the higher-order thermoelectric coefficients. The presence of a non-zero temperature gradient in a conducting medium directed perpendicular to the direction of a magnetic field gives rise to the Nernst coefficient. It measures the electric current perpendicular to both the magnetic field and the temperature gradient. In the absence of a magnetic field, this coefficient vanishes. The temperature dependence of the Nernst coefficient in the medium further gives rise to the transverse Thomson coefficient Th_N as shown in Eq. (77). Fig. 3 represents Th_N as a function of T for three different values of μ_B at 0.10, 0.30, and 0.40 GeV. The upper and lower panels present the results for the case of the magnetic field with values 0.1 and 1.0 m_π^2 , respectively. In the upper panel, we observe that Th_N is positive for lower values of T up to 0.11 GeV for $\mu_B = 0.10$ GeV. The positive values of Th_N signify that in Eq. (77), the quantity $2NB$ is dominating over the dynamical term, $T \frac{dNB}{dT}$ at lower temperatures. The impact of this dynamic part slowly starts increasing with T , and hence the negative behavior of Th_N is also observed at higher T . For the higher values of μ_B , it is observed that the dynamical part of Eq. (77) is dominating almost for the whole temperature range considered here. As it is observed in Ref. [13], the coefficient NB vanishes near high temperatures; here, Th_N also starts disappearing at higher temperatures. For $eB = 1.0 m_\pi^2$, results from different models are observed to be almost similar, i.e., no significant model dependence is observed. Even at higher μ_B , only a slight deviation in the models can be seen. As one goes to a higher value of the magnetic field ($eB = 1.0 m_\pi^2$), Th_N is observed to be higher. Due to the higher order of magnitude of σ_{el}/T as compare to σ_H/T , NB can be approximated by ratio $(\mathcal{I}_{42}/T^2)/(\sigma_{el}/T)$. The sharp decrease of \mathcal{I}_{42}/T^2 as compare to σ_{el}/T give rise to decreasing trend of NB with μ_B . Though NB decreases with increasing μ_B but the dynamical rate of decrease of NB increases. Hence, the coefficient Th_N mostly has negative values throughout the whole temperature range at high values of μ_B . For the case of high $\mu_B = 0.40$ GeV, a clear effect of magnetic field values can be observed in the upper and bottom panels of Fig. 3. As the magnetic field increases by a factor of 10, the transverse Thomson coefficient also increases by a factor of 10. This can be understood as for the larger values of μ_B , the baryons exceed the antibaryons on a large scale, the net charge in the system also increases. Hence, for the case of higher magnetic field, the effect of the Lorentz force is also high. Thus, the higher Lorentz force increases the thermoelectric effects in the transverse direction, which results in higher values of transverse Thomson coefficient. Once this magnetic field vanishes, the coefficient Th_N drops to zero only.

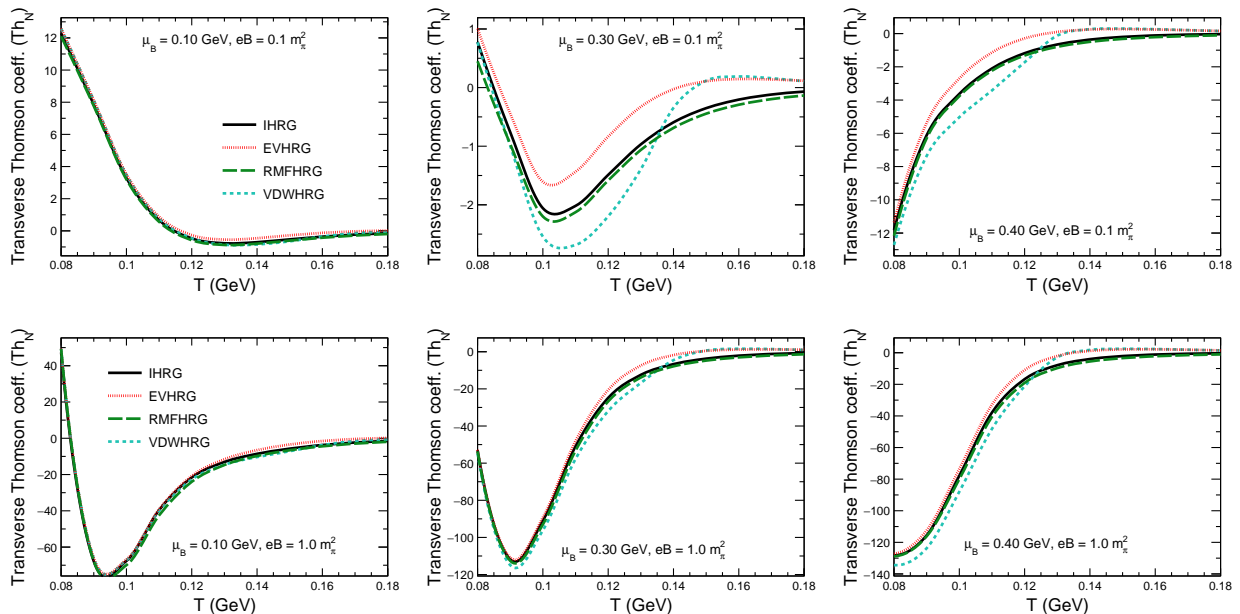


FIG. 3: Transverse Thomson coefficient (Th_N) as a function of temperature at magnetic field $eB = 0.1 m_\pi^2$ (upper panel) and $eB = 1.0 m_\pi^2$ (lower panel) for baryon chemical potential at $\mu_B = 0.10$ GeV (left), 0.30 GeV (middle), and 0.40 GeV (right).

IV. SUMMARY

In heavy-ion collisions, temperature gradients between the central and peripheral regions of the created fireball, especially in the presence of a non-zero baryon chemical potential, can introduce thermoelectric effects within the hot hadronic medium. The presence of a magnetic field induces anisotropy in the system by breaking rotational symmetry, enhancing direction-dependent thermoelectric responses. In this work, for the first time, we estimate the magneto-Thomson and transverse Thomson coefficients using different HRG models in the presence of a magnetic field. These higher-order thermoelectric coefficients arise from the temperature dependence of the leading-order thermoelectric coefficients. The Thomson coefficient quantifies the net generation or absorption of heat in the medium when current flows in the medium in the presence of a temperature gradient. We have studied this phenomenon in the presence of an external magnetic field. Here, the baryon conservation is considered for the heat conduction in the hot hadronic medium. Using the Gibbs-Duhem relation, we relate the gradients in baryon chemical potential to those in temperature, revealing the role of enthalpy in modifying the thermoelectric coefficients. The net leading-order thermoelectric coefficient vanishes for mesons due to their charge symmetry; mesons still have a significant effect on the leading-order thermoelectric coefficients because of their contributions to enthalpy. Furthermore, we explore the effect of different values of external magnetic fields on these transport properties. It is observed that

in the presence of a higher magnetic field ($eB = 1.0 m_\pi^2$), both the Th_B and Th_N show higher values as compared to lower values of magnetic field ($eB = 0.1 m_\pi^2$). It is also observed that for both the coefficients, the effect of different models is mostly significant at higher temperatures. The results for all four models almost overlap at the lower temperatures. In the absence of a magnetic field, the magneto-Thomson coefficient Th_B reduces to the Thomson coefficient Th . On the other hand, the transverse Thomson coefficient Th_N completely vanishes in the absence of a magnetic field because of the vanishing Lorentz force. Recently, both phenomena have also been studied in Ref. [62] for the QGP medium in detail using the quasi-particle approach.

In the domain of spintronics, which includes both the charge and spin degrees of freedom of electrons for next-generation information processing technologies, the Thomson coefficient plays a fundamental role in uncovering spin-dependent thermoelectric phenomena. A specialized subfield, spin-caloritronics, focuses on the influence of temperature gradients on spin currents and magnetization dynamics [64]. For instance, Ref. [65] discusses the generation of spin currents via the spin Hall effect, wherein a transverse spin current is induced in response to an electric field, analogous to the conventional Hall effect. Notably, thermoelectric-induced electric fields [12] can also contribute to the spin Hall current, establishing a direct link between thermal transport and spin dynamics. Recent experimental studies have further revealed the existence of a transverse Thomson effect in semimetallic alloys [33], highlighting the complex coupling between

thermal gradients, charge transport, and magnetization. This motivates exploration of similar phenomena in the hot and dense QCD medium, where effects such as spontaneous magnetization may give rise to an anomalous transverse Thomson effect, an area yet to be investigated in the context of heavy-ion collisions. Therefore, a comprehensive understanding of higher-order thermoelectric phenomena in the hot QCD medium is not only crucial for studying transport properties but also essential for studying emergent spin-related effects, including the spin Hall effect and spin polarization phenomena [66]. Overall, this study presents a detailed investigation of the higher-order thermoelectric properties of hot and dense hadronic matter within different HRG frameworks, emphasizing the impact of hadronic interactions and magnetic fields.

ACKNOWLEDGEMENT

KS and KKP acknowledge the financial aid from the University Grant Commission, Government of India. The authors gratefully acknowledge the DAE-DST, Govt. of India funding under the mega-science project – “Indian participation in the ALICE experiment at CERN” bearing Project No. SR/MF/PS-02/2021- IITI (E-37123).

-
- [1] W. Busza, K. Rajagopal and W. van der Schee, *Ann. Rev. Nucl. Part. Sci.* **68**, 339 (2018).
- [2] J. Brewer, L. Yan and Y. Yin, *Phys. Lett. B* **816**, 136189 (2021).
- [3] H.J. Goldsmid, *Introduction to Thermoelectricity*. Springer-Verlag Berlin Heidelberg, 2009.
- [4] K. Singh, J. Dey, R. Sahoo and S. Ghosh, *Phys. Rev. D* **108**, 094007 (2023).
- [5] K. Singh, J. Dey and R. Sahoo, *Phys. Rev. D* **109**, 014018 (2024).
- [6] Y. Wang, Y. Hu, S. Shang, B. Zhou, Z. Liu, & L. Chen. *Phys. Rev. B.* **98**, 224101 (2017)
- [7] J. Cai, and G. Mahan. *Phys. Rev. B.* **74**, 075201 (2006).
- [8] F. Spathelf, B. Fauqué, and K. Behnia. *Phys. Rev. B.* **105**, 235116 (2022).
- [9] J. Young, *Proc. Phys. Soc. London*, **37**, 145 (1924).
- [10] D.K.C. MacDonald, *Thermoelectricity: An Introduction to the Principles*, Dover Publications, Inc., New York, (2006).
- [11] K. Morrison and F. K. Dejene, *Physics*, **13**, 137 (2020).
- [12] K. Singh, J. Dey and R. Sahoo, *Phys. Rev. D* **110**, 114051 (2024).
- [13] K. Singh, K. K. Pradhan, D. Sahu and R. Sahoo, *Phys. Rev. D* **111**, 074033 (2025).
- [14] J. R. Bhatt, A. Das and H. Mishra, *Phys. Rev. D* **99**, 014015 (2019).
- [15] A. Das and H. Mishra, *Eur. Phys. J. ST* **230**, 607 (2021).
- [16] A. Das, H. Mishra and R. K. Mohapatra, *Phys. Rev. D* **102**, 014030 (2020).
- [17] M. Greif, J. A. Fotakis, G. S. Denicol and C. Greiner, *Phys. Rev. Lett.* **120**, 242301 (2018).
- [18] M. Prakash, R. Venugopalan and G. Welke, *Phys. Rept.* **227**, 321 (1993).
- [19] G. Kadam, *Mod. Phys. Lett. A* **30**, 1550031 (2015).
- [20] H. Meyer, *Eur. Phys. J. A.* **47** (2011).
- [21] O. Kaczmarek and H. T. Shu, *Lect. Notes Phys.* **999**, 307 (2022)
- [22] X. Wang, and I. Shovkovy, *Eur. Phys. J. C.* **81**, 901 (2021).
- [23] B. McInnes, *Nuclear Physics B.* **911**, 173 (2016).
- [24] J. Dey, A. Bandyopadhyay, A. Gupta, N. Pujari, & S. Ghosh, *Nuclear Physics A.* **1034**, 122654 (2023).
- [25] K. Gowthama, M. Kurian, and V. Chandra, *Phys. Rev. D.* **106**, 034008 (2022).
- [26] K. Gowthama, M. Kurian, and V. Chandra, *Phys. Rev. D.* **104**, 094037 (2021).
- [27] H. X. Zhang, K. M. Shen, Y. X. Xiao and B. W. Zhang, *Phys. Rev. D* **110**, 034023 (2024).
- [28] A. Abhishek, A. Das, D. Kumar and H. Mishra, *Eur. Phys. J. C* **82**, 71 (2022).
- [29] M. Kurian, *Phys. Rev. D* **103**, 054024 (2021).
- [30] H. X. Zhang, J. W. Kang and B. W. Zhang, *Eur. Phys. J. C* **81**, 623 (2021).
- [31] Y. Kimura, K. Utsumi, and H. Tohmyoh, *Appl. Therm. Eng.*, **255**, 124009, (2024).
- [32] K. Uchida, M. Murata, A. Miura, and A. Iguchi, *Phys. Rev. Lett.* **125**, 106601 (2020).
- [33] A. Takahagi, T. Hirai, A. Alasli, S. Park, H. Nagano, and K. Uchida, *arXiv:2501.05857 Nat. Phys.* (2025).
- [34] R. Bellwied, S. Borsanyi, Z. Fodor, S. D. Katz and C. Ratti, *Phys. Rev. Lett.* **111**, 202302 (2013).
- [35] R. Bellwied, S. Borsanyi, *et al.* *Nucl. Phys. A* **967**, 732 (2017).
- [36] S. Borsanyi, Z. Fodor, C. Hoelbling, S. D. Katz, S. Krieg and K. K. Szabo, *Phys. Lett. B* **730**, 99 (2014).
- [37] A. Bazavov *et al.* [HotQCD], *Phys. Rev. D* **90**, 094503 (2014).
- [38] A. Bazavov, H. T. Ding, P. Hegde, O. Kaczmarek, F. Karsch, E. Laermann, Y. Maezawa, S. Mukherjee, H. Ohno and P. Petreczky, *et al.* *Phys. Rev. Lett.* **111**, 082301 (2013).
- [39] A. Bazavov, H. T. Ding, P. Hegde, O. Kaczmarek, F. Karsch, E. Laermann, Y. Maezawa, S. Mukherjee, H. Ohno and P. Petreczky, *et al.* *Phys. Rev. D* **95**, 054504 (2017).
- [40] S. Borsanyi, Z. Fodor, J. N. Guenther, S. K. Katz, K. K. Szabo, A. Pasztor, I. Portillo and C. Ratti, *JHEP* **10**, 205 (2018).
- [41] A. Andronic, P. Braun-Munzinger, J. Stachel and M. Winn, *Phys. Lett. B* **718**, 80 (2012).

- [42] G. P. Kadam, H. Mishra and L. Thakur, Phys. Rev. D **98**, 114001 (2018).
- [43] G. P. Kadam and H. Mishra, Phys. Rev. C **92**, 035203 (2015).
- [44] S. Pal, G. Kadam, H. Mishra and A. Bhattacharyya, Phys. Rev. D **103**, 054015 (2021).
- [45] J. I. Kapusta and K. A. Olive, Nucl. Phys. A **408**, 478 (1983).
- [46] K. A. Olive, Nucl. Phys. B **190**, 483 (1981).
- [47] V. Vovchenko, Phys. Rev. C **96**, 015206 (2017).
- [48] V. Vovchenko, M. I. Gorenstein and H. Stoecker, Phys. Rev. Lett. **118**, 182301 (2017).
- [49] S. Samanta and B. Mohanty, Phys. Rev. C **97**, 015201 (2018).
- [50] V. Vovchenko, D. V. Anchishkin and M. I. Gorenstein, Phys. Rev. C **91**, 064314 (2015).
- [51] C. Amsler *et al.* [Particle Data Group], Phys. Lett. B **667**, 1 (2008).
- [52] K. K. Pradhan, D. Sahu, R. Scaria and R. Sahoo, Phys. Rev. C **107**, 014910 (2023).
- [53] D. H. Rischke, M. I. Gorenstein, H. Stoecker and W. Greiner, Z. Phys. C **51**, 485 (1991).
- [54] A. Bhattacharyya, S. Das, S. K. Ghosh, R. Ray and S. Samanta, Phys. Rev. C **90**, 034909 (2014).
- [55] V. Vovchenko, D. V. Anchishkin, M. I. Gorenstein and R. V. Poberezhnyuk, Phys. Rev. C **92**, 054901 (2015).
- [56] N. Sarkar and P. Ghosh, Phys. Rev. C **98**, 014907 (2018).
- [57] P. Huovinen and P. Petreczky, Phys. Lett. B **777**, 125 (2018).
- [58] G. Kadam and H. Mishra, Phys. Rev. D **100**, 074015 (2019).
- [59] P. Huovinen, and P. Petreczky, Phys. Lett. B. **777** 125 (2018).
- [60] S. Gavin, Nucl. Phys. A **435**, 826 (1985).
- [61] A. F. Ioffe, Physics of semiconductors, Foreign Languages Publishing House, Moscow (1957).
- [62] K. Singh and R. Sahoo, [arXiv:2504.21734 [hep-ph]].
- [63] A. Das, H. Mishra and R. K. Mohapatra, Phys. Rev. D **99**, 094031 (2019).
- [64] I. Starkov, O. Pakhomov and A. Starkov Journal Of Magnetism And Magnetic Materials, **496** (2020).
- [65] S. Y. F. Liu and Y. Yin, Phys. Rev. D **104**, 054043 (2021).
- [66] S. Singha, EPJ Web Conf. **276**, 06012 (2023).